SAND2016-12803C

S51A-2744

liam.toney@pomona.edu

Surface-wave tomography of Yucca Flat, Nevada

Liam D. Toney[1,2], Robert E. Abbott[2], Hunter A. Knox[2], Leiph A. Preston[2], Charles R. Hoots[2]

1. Pomona College, Claremont, CA
2. Sandia National Laboratories, Albuquerque, NM

Background

In 2015, Sandia National Laboratories conducted an active-source seismic survey of Yucca Flat, Nevada, on the Nevada National Security Site (NNSS). Data from this survey will help characterize seismic propagation effects of the area, informing models for the next phase of the Source Physics Experiment (SPE). SPE consists of a series of intensively monitored chemical detonations emplaced in various geologies on the NNSS. The goal of SPE is the successful development of a physics-based predictive capability for detecting small nuclear detonations under the Comprehensive Test Ban Treaty.

Yucca Flat is a Tertiary extensional basin with a basement primarily composed of Paleozoic carbonate rocks. A thick layer of alluvial and volcanic deposits resides within the basin; this layer is greater than 1 km in thickness in the deepest areas of the basin [*Phelps et al.*, 2011]. The next phase of SPE will take place in this unconsolidated alluvial setting, in contrast to the granitic geology of the previous phase. Yucca Flat hosted over 900 nuclear tests between 1951 and 1992; the effects of these detonations on the shallow and surface geology make Yucca Flat a very unique and interesting survey location.

The 2015 seismic survey consisted of two intersecting transects: THOR 1, a 19-km line oriented roughly north-south; and THOR 2, a 11-km line oriented roughly east-west. The detonations for the next phase of SPE will be located at the intersection of the two transects.

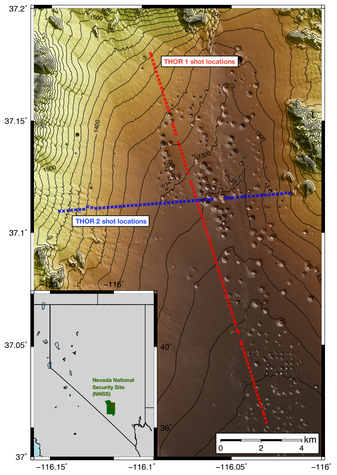

Fig. 1 *Survey location and geometry.*

Data acquisition

The survey source was the Seismic Hammer™, a 13,000-kg modified industrial pile driver. This massive weight-drop source struck the ground at 200 m intervals along both transects: 91 locations along THOR 1, and 56 locations along THOR 2. There were 32 strikes at each shot location to ensure a robust signal-to-noise ratio (SNR).

Over 350 three-component 2-Hz geophones were variably spaced at 10, 20, and 100 m along each line. We employed roll-along survey geometry to ensure 10-m receiver spacing within 2 km of the source for each shot location (Figure 3).

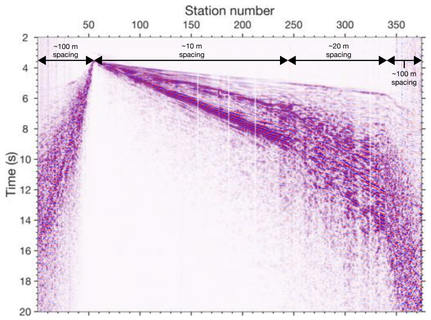

Fig. 3 *Shot gather from THOR 1, illustrating variable station spacing.*

Fig. 2 *Seismic Hammer™ at Yucca Flat.*

The data exhibits a very strong SNR due to the high-energy source and the large size of the fold. As illustrated in Figure 3, there is usable data out to greater than 4-km offsets.

All shot gathers exhibit a strong precursor occurring approximately 0.5 s before the initial hammer impact. This is identified as ground elastic rebound, caused by the 13,000-kg mass unloading the surface as it free-falls 1.5 m before impacting the hammer plate.

Multiple filter technique

We utilized the multiple filter technique (MFT) [*Dziewonski et al.*, 1969] to construct group velocity dispersion curves from the data:

1. We created a series of 30 Gaussian band-pass filters of constant relative bandwidth with center frequencies logarithmically spaced between 1 and 50 Hz.
2. We performed the following on every trace for each of the 30 frequency bands:
   i. Detrend, taper, and filter the trace.
   ii. Take the Hilbert transform to obtain the analytic signal amplitude (envelope) and instantaneous frequency.
   iii. Pick envelope local maxima. These are interpreted as fundamental and higher-mode Rayleigh wave arrivals.

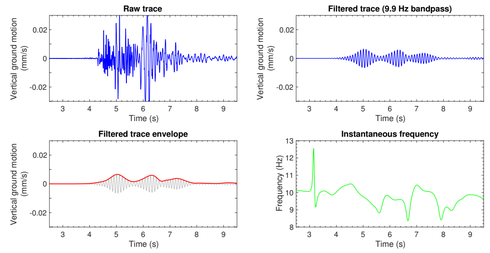

Fig. 4 *Workflow for multiple filter technique.*

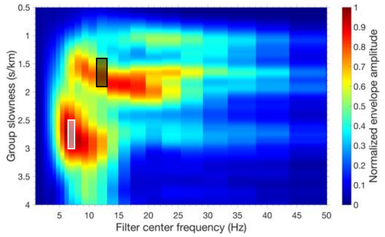

Fig. 5 *Time-frequency analysis of a single trace. Black and white boxes delineate trace sections sampled by hodograms below.*

The resultant envelopes can be visualized by a time-frequency analysis plot of the filtered trace. Figure 5 displays the 30 filtered envelopes from a single trace of THOR 1. The vertical time axis has been converted to slowness using the known source-receiver offset. Warmer colors indicate larger amplitudes. Plots such as these highlight the dispersion in the surface wave data.

Two dispersive elements are evident in Figure 5. We initially interpreted these as the Rayleigh fundamental and first higher mode. However, the lower-velocity, narrower-bandwidth element contains a large portion of energy in the vicinity of 2.8-3.0 s/km (333-357 m/s). We hypothesized that this slower feature was in fact a ground-coupled airwave, as opposed to the fundamental Rayleigh wave arrival.

Inversion preparation

We utilized hodogram analysis to differentiate between the two observed dispersive features.

The hodogram in Figure 6a is derived from the region of the suspected airwave. Particle motion is prograde and near-circular; the prograde motion indicates that this signal is not a fundamental Rayleigh wave.

In Figure 6b, the hodogram is derived from the region of the suspected fundamental Rayleigh arrival. Particle motion is retrograde elliptical, which is characteristic of Rayleigh waves.

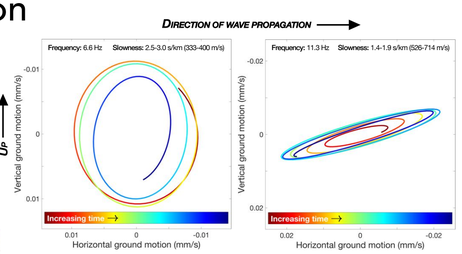

Fig. 6a *Hodogram created from white boxed region (airwave).*

Fig. 6b *Hodogram created from black boxed region (Rayleigh wave).*

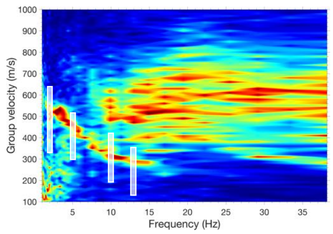

Fig. 7 *Plot of all envelope maxima picks for a single shot. Warmer colors signify more picks in that frequency-velocity region. White boxes denote velocity windows at that frequency (not all windows are shown above).*

The picks generated in step 2 of the MFT workflow described above contain higher mode and airwave arrivals in addition to the desired fundamental Rayleigh arrivals. However, our inversion code utilizes only fundamental Rayleigh picks. It was therefore necessary to isolate the fundamental Rayleigh dispersion curve from other data features.

To accomplish this, we created generalized dispersion curve plots for each shot of THOR 1 and THOR 2. Figure 7 illustrates this type of plot. After visual identification of the fundamental Rayleigh dispersion curve, we created velocity windows for each frequency band. We subsequently used these windows to remove spurious picks.

The dispersion evident in Figure 7 is very well-defined. However, some shots exhibited anomalies in both the frequency and velocity domains which resulted in very poorly-defined dispersion curves. Such shots were processed with arbitrarily wide velocity windows.

Results and interpretation

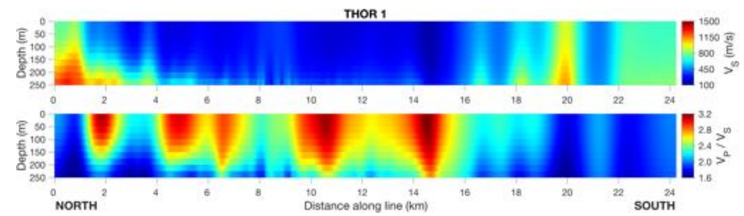

Fig. 8 *THOR 1, 2-D shear-wave velocity and V_P / V_S ratio. V_P values from Tang and Abbott [2015].*

We executed a joint inversion for shear- and compressional-wave velocities utilizing Sandia's internal "tomag" code. Initial tomography results for THOR 1 are shown in Figure 8. In the northern third of the transect, the region of slow (<500 m/s) shear-wave velocity generally becomes deeper towards the south. This is consistent with groundtruth from borehole logs and gravity surveys (Figure 10); an alluvial (slow) layer thickens towards the south in the corresponding section of the geologic model.

The V_P / V_S ratio along the THOR 1 transect exhibits anomalously large values in five distinct regions. Since we expect V_P / V_S ratio to increase as pore space increases, these anomalies may indicate the presence of disrupted alluvium: Material which may have been significantly disturbed following a nuclear test detonation. Further comparison with known chimney locations is required to verify this potential explanation.

Additionally, large V_P / V_S ratio materials are conducive to the presence of leaky compressional-wave modes, and such dispersive "P_L" features are visible on refraction microtremor (ReMi) plots derived from THOR phase velocity picks. This observation reinforces the notion that our anomalous V_P / V_S ratios represent a physical feature of the subsurface as opposed to an inversion artifact.

The THOR 2 inversion process is still ongoing. However, the dispersion curve picks for THOR 2 extend significantly higher in frequency than those for THOR 1 (Figure 9); this will improve the shallow-depth resolution of the resultant velocity model.

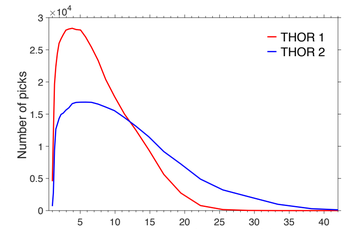

Fig. 9 *Total number of inverted picks per frequency band for THOR 1 and THOR 2. THOR 2 picks exhibit a significantly broader bandwidth.*

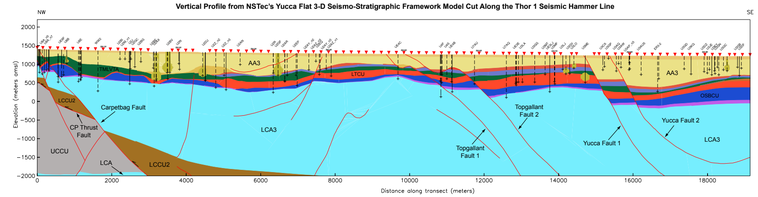

Fig. 10 *Geologic cross-section underneath the THOR 1 line. Figure courtesy of Lance Prothro, NSTec.*

References

Dziewonski, A., S. Bloch, and M. Landisman (1969), A technique for the analysis of transient seismic signals, *Bull. Seismol. Soc. Am.*, 59, 427–444.

Phelps, G. A., A. Boucher, and K. J. Halford (2011), A refined characterization of the alluvial geology of Yucca Flat and its effect on bulk hydraulic conductivity, *Open-File Rep. 2010-1307*, U.S. Geol. Surv., Menlo Park, Calif.

Tang, D. G., and R. E. Abbott (2015), Hammering Yucca Flat, part one: P-wave velocity, Abstract S53B-2808 presented at 2015 Fall Meeting, AGU, San Francisco, Calif., 14-18 Dec.

Acknowledgements

We thank the following people for their invaluable contributions to the THOR project:

Lance Prothro, Sig Drellack, and Maggie Townsend (Geology, NSTec); Bob White, Frank Spenia, and Jesse Bonner (Operations, NSTec); Ping Lee (Program Facilitator, DRI)

This work was funded by the NNSA under the Source Physics Experiment program.